VERTICAL DISTRIBUTION OF OZONE, AS MEASURED BY SPICAM ON MARS-EXPRESS.

S. Lebonnois, *Laboratoire de Météorologie Dynamique/IPSL, Paris, France (Sebastien.Lebonnois@lmd.jussieu.fr)*, **E. Quemerais, F. Montmessin, F. Lefèvre, S. Perrier, J.-L. Bertaux,** *Service D'Aéronomie/IPSL, Verrières-le-Buisson, France*, **F. Forget,** *Laboratoire de Météorologie Dynamique/IPSL, Paris, France*.

Introduction

The SPICAM instrument onboard the european Mars-Express mission is an ultraviolet and infrared spectrometer working in the ranges [118-300] nm and [1.0-1.7] μm and dedicated to the study of the atmosphere and ionosphere of Mars (*Bertaux et al.*, 2000, 2005). The UV channel modes include nadir viewing, limb viewing and vertical profiling of the atmosphere by stellar or solar occultations. The IR channel is dedicated primarily to nadir measurements of the water vapor abundances, vertical profiling of water vapor and aerosols during solar occultations, and detection of 1.27 μm $O_2(^1\Delta_g)$ emissions (*Korablev et al.*, 2002).

Among its scientific objectives, SPICAM can determine and monitor the ozone (O_3) distribution in the atmosphere of Mars. Ozone was detected in the Martian atmosphere by the Mariner 7 (1969) and 9 (1971-1972) ultraviolet spectrometers (*Barth and Hord*, 1971; *Barth et al.*, 1973). It has since been observed both directly at Mars, including some tentatives of vertical profiling, (Mars 5 and Phobos 2 spacecraft, *Krasnopolsky and Parshev* (1979); *Blamont and Chassefière* (1993)), and from Earth (*Espenak et al.*, 1991; *Clancy et al.*, 1996, 1999; *Novak et al.*, 2002; *Fast et al.*, 2005). With its different modes, SPICAM can retrieve atmospheric ozone using three distinct methods: (1) in nadir geometry, the Hartley O_3 absorption band at 250 nm is detected in the solar spectrum scattered back from the ground, which allows to retrieve the ozone column abundance in the atmosphere; (2) during stellar and solar occultations, the same absorption band is seen in the transmission spectrum, giving access to the ozone abundance along the line of sight, as a function of altitude; (3) in the infrared, the O_2 airglow at 1.27 μm is emitted through relaxation of $O_2(^1\Delta_g)$ excited molecules, which are produced by photodissociation of ozone molecules by solar UV photons, providing a measure of ozone above approximately 20 km altitude, level below which the $O_2(^1\Delta_g)$ molecules are quenched by CO_2 collisions.

In this presentation, we will discuss the second method, using the UV signature of ozone in the transmission spectra that have been obtained during stellar occultations. Up to now, only models have been giving insights into the vertical distribution of ozone, and its behaviour as a function of latitude and season (*Clancy and Nair*, 1996; *Lefèvre et al.*, 2004). The SPICAM dataset of stellar occultations gives a unique opportunity to explore this in depth.

Data Analysis

During a stellar occultation, SPICAM UV field of view is pointed toward a star, and its detector records the stellar spectrum as the spacecraft drifts on its orbit and the star rises or sets behind the atmosphere of Mars. From January 2004 to mid-August 2005, 629 stellar occultations have been done with SPICAM, among which 433 have been successfully analyzed to retrieve ozone vertical profiles. This set of vertical profiles covers solar longitudes from 8.3° (just after northern spring equinox) to 270° (northern winter solstice).

The method used here is a self-calibrated method, that does not need absolute calibration of the stellar spectra. The range [120-280] nm is used in order to retrieve CO_2 and O_3 densities along the line of sight (slant densities), as well as aerosols (dust and/or clouds) opacities and spectral behaviour. First, a reference spectrum of the star outside the atmosphere is computed from spectra measured above 180 km altitude, then all spectra during the occultation are ratioed to this reference stellar spectrum, to get atmospheric transmission spectra as a function of the altitude of the tangential point above a reference ellipsoid. For the following study, altitudes are adjusted to the MOLA topography reference. Therefore, altitudes quoted in this paper are not the actual altitudes above the surface of Mars.

Wavelengths shortward of 200 nm are used to retrieve CO_2 slant densities, aerosols opacities are affecting the whole spectrum, and longward of 200 nm, the transmission spectra are dominated by CO_2 Rayleigh extinction with an additional trough around 250 nm due to the O_3 absorption band (Fig. 1). The depth of this trough is a measure of the ozone slant density, which is then retrieved as a function of altitude. Given the S/N ratio obtained in the stellar occultations, ozone is detected for column densities larger than approximately 10^{15} molecules cm^{-2}, a value that was expected from simulations performed before the mission (*Korablev et al.*, 2001). Associated error bars are of the order of 1 to 5×10^{15} molecules cm^{-2}.

The vertical profile of slant densities of CO_2 and O_3 are then inverted with an "onion peeling" procedure to get their vertical density profiles. This procedure includes a Tikhonov regularization method to avoid amplification of the noise of the slant densities data. This improves the vertical profile, but reduces the vertical resolution, which is typically around 5 km, up to 10 km for the most noisy cases. Depending on the dust opacity,

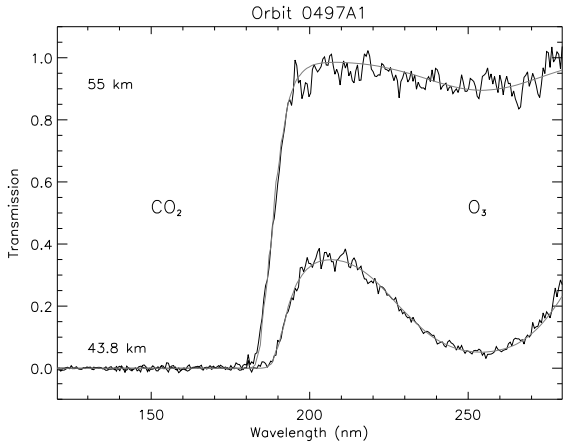

Figure 1: Example of a transmission spectra, for orbit 497A1 (latitude = 29.7°S, longitude = 105.7°E, local time = 21h, solar longitude = 45.5°). Two altitudes are shown: 55.0 and 43.8 km. The calculated fits shown here includes the column densities along the line of sight N_{CO_2} and N_{O_3}, and dust parameters: opacity at 250 nm τ and and Angström coefficient α ($\tau_{dust} = k\lambda^{-\alpha}$). Values for 55 km altitude are: N_{CO_2} = 1.35×10^{22} molecules cm^{-2} N_{O_3} = 9.28×10^{15} molecules cm^{-2}, τ = 0., and α = 1.; and values for 43.8 km are: N_{CO_2} = 4.66×10^{22} molecules cm^{-2} N_{O_3} = 1.93×10^{17} molecules cm^{-2}, τ = 0.35, and α = 1.1085.

the CO_2 density is retrieved down to the altitude where the stellar signal is lost completely, typically 20-30 km. We use this lowest altitude for CO_2 density retrieval as the lower boundary for the ozone density retrieval. The upper boundary for the ozone retrieval procedure is fixed at 80 km altitude, with no signal usually detected above 60-70 km. The detection limit for ozone abundance is approximately 10^8 molecules cm^{-3}, with usual error bars of the order of 10^8 to 10^9 molecules cm^{-3}.

Distribution of the Nocturnal Ozone Layer

Mid- and Low-latitudes

The first stellar occultations monitored by SPICAM, and useful for this study, occurred at $L_s = 8°$ (right after northern spring equinox). SPICAM probed northern mid-latitudes (latitudes between 30 and 60°N) until L_s = 24°. Then, measurements were mostly performed in the tropical region ($L_s = 10°$ to 50° for latitudes between 0 and 30°N, $L_s = 30°$ to 80° for latitudes between 0 and 30°S). During the second half of southern autumn ($L_s = 45°$ to 80°), SPICAM stellar occultations also probed southern mid-latitudes (between 30 and 60°S).

No ozone layer is detected during the first occultations, in northern mid-latitudes, though the occultations probed down to roughly 30 km altitude, even down to 20 km in some cases. The upper limit due to error bars is a few 10^8 cm^{-3}. Closer to equator, the lower limit of the retrieved profiles is around 35 km altitude. The first ozone layer is detected on orbit 247 ($L_s = 11.0°$, 2.3°E, 16.8°N), at 52 km altitude, with a peak abundance of $(4.7\pm0.7)\times10^8$ cm^{-3}. For $L_s = 28°$ to 40°, both north and south of the equator, an ozone layer is systematically observed between 35 and 50 km altitude, with a peak abundance of 1-4$\times10^9$ cm^{-3} in northern tropics, located around 45 km (slighty lower for southern latitudes), and of 2-3$\times10^9$ cm^{-3} in southern tropics. After mid-autumn, the peak altitude tends to be slighly lower, around 40 km, and its abundance increases up to 6-9$\times10^9$ cm^{-3}. This is the aphelion season, with apoapsis reach around $L_s = 71°$. For southern mid-latitudes, the ozone layer is also present during the second half of autumn, with similar characteristics, though it appears thicker than in the tropics (present between 25-30 and 50 km altitude), and with a peak abundance varying between 4-8$\times10^9$ cm^{-3}.

Moving into southern winter ($L_s = 93°$ to 180°), the observed ozone layer evolves with the season, depending on the latitude. During this season, probed latitudes have been mostly located in the southern hemisphere. At low latitudes (0 to 30°S), the occultations probe down to 20-30 km altitude until $L_s \sim 130°$, then the aerosol opacity in the lower atmosphere tends to increase, and the lower limit gets higher, around 35-40 km. During early winter ($L_s = 93°$ to 110°), the layer is still thick, between 25 and 45-50 km altitude, with a broad peak around 35-40 km of 5-8$\times10^9$ cm^{-3}, decreasing to $\sim 4\times10^9$ cm^{-3} after $L_s = 100°$. In this layer, double peaks are often observed. After $L_s = 110°$, ozone is only barely detected on a few orbits, even when the lower limit gets down to 30 km.

In mid latitudes (30 to 60°S), this decrease in the ozone layer abundance with time is also observed. Between $L_s = 94°$ and 122°, the occultations probe very deep, even down to 10 km altitude for many orbits. A broad ozone layer is observed between 30 and 50 km altitude, with a peak abundance decreasing from $\sim 6\times10^9$ cm^{-3} before $L_s = 105°$ to 2-3$\times10^9$ cm^{-3} until $L_s = 122°$. Structures in the layer are seen on a few profiles. Between $L_s = 122°$ and 133°, the ozone layer is still observed between 25 and 50 km altitude, with a peak around 40$\pm$5 km, but with lower abundance, less than 2×10^9 cm^{-3}. After $L_s = 133°$, the probing lower limit becomes highly variable, located between 30 and 60 km altitude. Similarly to low latitudes, no more ozone is detected at this season.

Between northern fall equinox and northern winter solstice, occultations have been performed for latitudes ranging from 30°S to 60°N, with only 3 occultations in the northern polar region. Probing lower limit varies from 50 to 20 km, but no ozone layer is detected at this season for any latitude.

Figure 2 summarizes all the vertical profiles of ozone

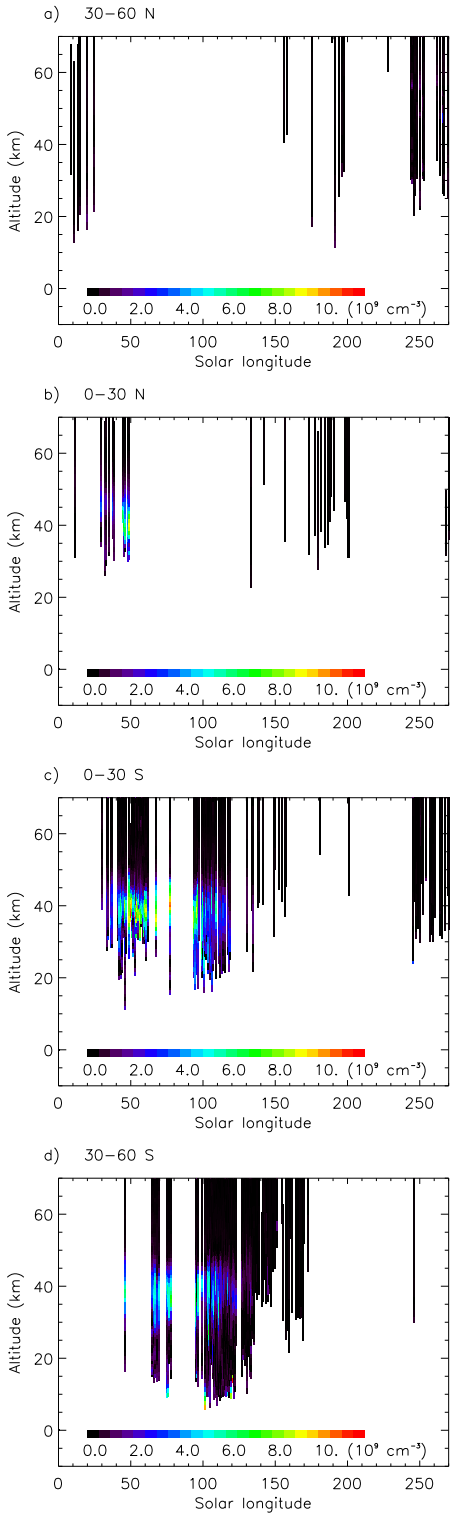

Figure 2: Seasonal evolution of the ozone abundance in the nocturnal layer observed by SPICAM, for different latitude ranges (mid- and low-latitudes, unit is 10^9 cm^{-3}).

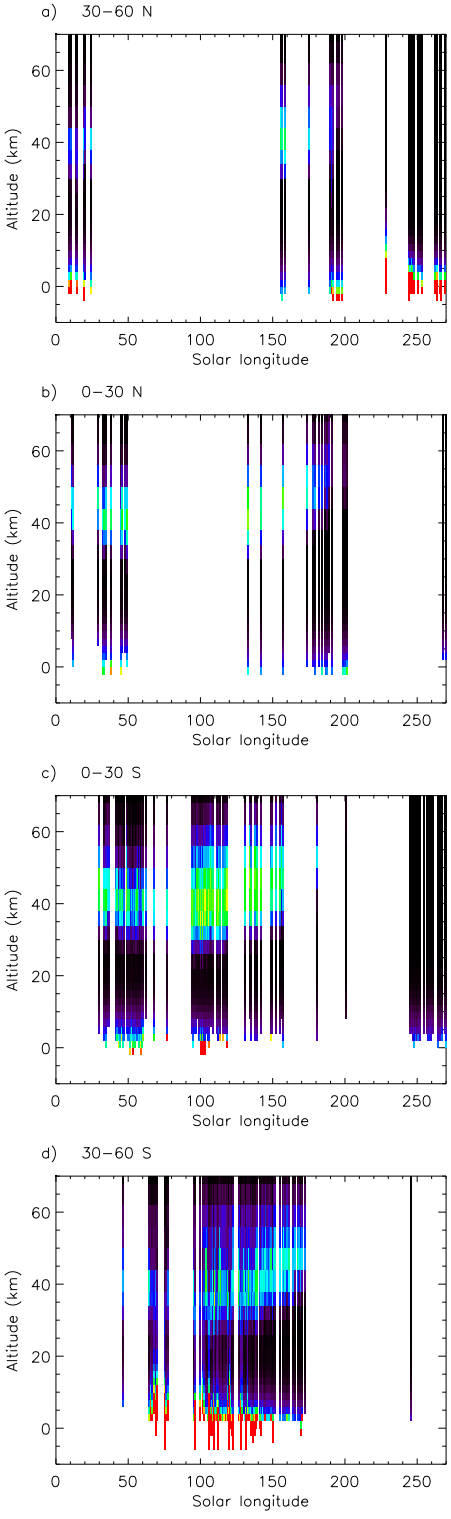

Figure 3: Abundances predicted in the General Circulation Model at the same location and season as observations (Fig. 2 and 4), from the surface up to 70 km altitude (unit and color scale is the same as for observed values).

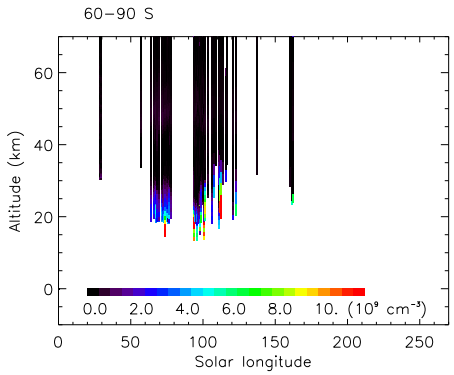

Figure 4: Same as Fig. 2, but for southern high-latitudes.

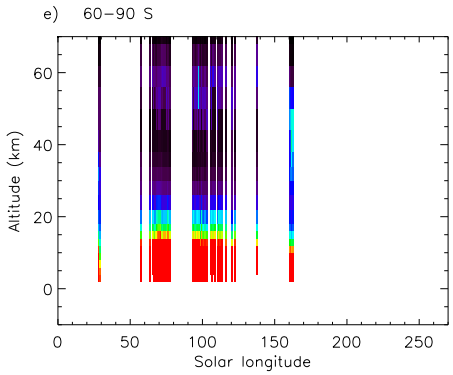

Figure 5: Same as Fig. 3 for high-latitudes (to be compared with Fig. 4.

observed for mid- and low-latitudes. The ozone layer appears essentially between $L_s \sim 40°$ and $L_s \sim 110°$, season which is approximately centered on the aphelion ($L_s = 71°$).

Southern High Latitudes

Latitudes poleward of 60°S have been probed in late autumn and winter, between $L_s = 56°$ and 162°.

The lowest altitude of the profiles is located between 15 and 30 km. A small ozone layer is observed in the altitude range 40 to 60 km, with a peak altitude around 50 km, and an abundance of approximately 2-5$\times 10^8$ cm^{-3} (error bars are approximately 1×10^8 cm^{-3}), before $L_s \sim 125°$. No ozone is detected for the last six occultations, at $L_s = 136°$ and $L_s = 160 - 161°$, down to 25-30 km altitude. Two additionnal occultations obtained at $L_s = 28 - 29°$ and latitude 61.5 detected no ozone down to 35 km altitude, with a noise level around 2×10^8 cm^{-3}. Figure 4 summarizes all the vertical profiles of ozone observed for high-latitudes.

At lower altitudes, below 30 km, ozone abundance is rising with decreasing altitudes. According to the atmospheric model, this is consistent with the surface layer of ozone that was predicted in the winter polar region by *Lefèvre et al.* (2004), due to the depletion in atmospheric water vapor. On one third of the profiles reaching down to 20 km, some structure is visible in this layer, with a depletion of ozone around 20-25 km.

Comparison to Model

A nocturnal ozone layer was predicted by a coupled chemistry-transport 3-dimensional General Circulation Model (*Lefèvre et al.*, 2004) in the altitude range where SPICAM observed it. In Fig. 3 and 5 , the abundances predicted in the General Circulation Model are plotted the same way as in Fig. 2 and 4, using the same location and solar longitudes. In the period between $L_s \sim 40°$ and $L_s \sim 100 - 110°$, there is a general agreement between observations and modeled profiles, but the duration of the period during which this nocturnal ozone layer is present is much shorter in the SPICAM data than in the model. During the period where there is a good agreement, the thickness of the layer, the peak abundance and the peak altitude are well reproduced by the model in most cases.

Discussion

Several hypothesis may be considered to explain the discrepancy between modeled and observed ozone profiles for altitudes between 30 and 60 km. The observed season for this ozone layer is centered on the aphelion, as in the model, which corresponds to the minimum water vapor content in the atmosphere. Since water vapor plays a key role in the abundance of ozone in this region, through the available amount of HO_x radicals, it seems very likely that a slight shift in the temperature seasonal evolution of this region would induce differences in the water content, and therefore differences in ozone abundance. With the same set of SPICAM stellar occultations, temperature profiles can be retrieved, and compared with the GCM profiles, to see whether observed differences are compatible with this hypothesis.

The infrared channel is not available for stellar occultations, but SPICAM was designed to observe transmission through the atmosphere both in the ultraviolet (retrieving ozone) and in the infrared (retrieving water vapor) during solar occultations. This simultaneous observations of water and ozone profiles, when processing will be completed, should also tell more about the role of water vapor.

There may be possible influences of dust content in this altitude region. It can induce temperature changes, and therefore affect indirectly the water vapor content, and it can also have a direct influence on ozone through

potential heterogeneous reactions destroying ozone at the surface of dust particles. SPICAM stellar occultations also enable the monitoring of the dust opacity, but there are very few laboratory data that would help quantify such heterogeneous destruction of ozone.

Considering the lack of information on ozone vertical profiles that was available before this SPICAM dataset, the good agreement between model predicted profiles and observations is very encouraging, and should help validate our understanding of the ozone chemical cycle in the martian atmosphere.

References

Barth, C. A., and C. W. Hord (1971), Mariner ultraviolet spectrometer: topography and polar cap, *Science*, *173*(3993), 197–201.

Barth, C. A., C. W. Hord, A. I. Stewart, A. L. Lane, M. L. Duck, and G. P. Anderson (1973), Mariner 9 ultraviolet spectrometer experiment: seasonal variation of ozone on Mars, *Science*, *179*, 795–796.

Bertaux, J.-L., et al. (2000), The study of the martian atmosphere from top to bottom with SPICAM light on Mars Express, *Planet. & Space Sci.*, *48*(12-14), 1303–1320.

Bertaux, J.-L., et al. (2005), Global structure and composition of the martian atmosphere with SPICAM on Mars Express, *Adv. Space Res.*, *35*(1), 31–36.

Blamont, J. E., and E. Chassefière (1993), First detection of ozone in the middle atmosphere of Mars from solar occultation measurements, *Icarus*, *104*, 324–336.

Clancy, R. T., and H. Nair (1996), Annual (perihelion-aphelion) cycles in the photochemical behavior of the global Mars atmosphere, *J. Geophys. Res.*, *101*(E5), 12,785–12,790.

Clancy, R. T., A. W. Grossman, M. J. Wolff, P. B. James, Y. N. Billawala, B. J. Sandor, S. W. Lee, and D. J. Rudy (1996), Water vapor saturation at low altitudes around Mars aphelion: a key to Mars climate ?, *Icarus*, *122*, 36–62.

Clancy, R. T., M. J. Wolff, and P. B. James (1999), Minimal aerosol loading and global increases in atmospheric ozone during the 1996-1997 martian northern spring season, *Icarus*, *138*, 49–63.

Espenak, F., M. J. Mumma, T. Kostiuk, and D. Zipoy (1991), Ground-based infrared measurements of the global distribution of ozone in the atmosphere of Mars, *Icarus*, *92*, 252–262.

Fast, K., et al. (2005), Ozone abundance on Mars from infrared heterodyne spectra. I: Acquisition, retrieval, and anticorrelation with water vapor, *Icarus*, submitted.

Korablev, O., J.-L. Bertaux, and J.-P. Dubois (2001), Occultation of stars in the UV: study of the atmosphere of Mars, *J. Geophys. Res.*, *106*(E4), 7597–7610.

Korablev, O., J.-L. Bertaux, A. Grigoriev, E. Dimarellis, Y. Kalinnikov, A. Rodin, C. Muller, and D. Fonteyn (2002), An AOTF-based spectrometer for the studies of Mars atmosphere for Mars-Express mission, *Adv. Space Res.*, *29*(2), 143–150.

Krasnopolsky, V. A., and V. A. Parshev (1979), Ozone photochemistry of the martian lower atmosphere, *Planet. & Space Sci.*, *27*, 113–120.

Lefèvre, F., S. Lebonnois, F. Montmessin, and F. Forget (2004), Three-dimensional modeling of ozone on Mars, *J. Geophys. Res.*, *109*(E7), E07004, doi: 10.1029/2004JE002268.

Novak, R. E., M. J. Mumma, M. A. DiSanti, N. Dello Russo, and K. Magee-Sauer (2002), Mapping of ozone and water in the atmosphere of Mars near the 1997 aphelion, *Icarus*, *158*, 14–23.